Soft Matter

PAPER

View Article Online
View Journal

Cite this: DOI: 10.1039/d0sm01375g

Competing pathways for the invagination of clathrin-coated membranes

Felix Frey †[ab] and Ulrich S. Schwarz *[ab]

Received 28th July 2020,
Accepted 20th October 2020

DOI: 10.1039/d0sm01375g

rsc.li/soft-matter-journal

Clathrin-mediated endocytosis is the major pathway by which eukaryotic cells take up extracellular material, but it is still elusive which physical pathways are being taken during membrane invagination. From a continuum point of view, it can be driven by increases in coat stiffness, preferred curvature or line tension. Here we develop a comprehensive theoretical framework that can be solved analytically and that predicts the consequences of these different scenarios. We find that for the case of increasing stiffness or preferred curvature, curvature will be acquired gradually with growth, while for increasing line tension, the lattice must have grown to a certain size before a flat-to-curved transition can occur. At low membrane tension, the critical value for coat stiffness is 30 k_BT, for preferred curvature it is 200 nm, and for line tension it is 6 pN. For high membrane tension, critical coat stiffness is 150 k_BT and critical preferred curvature is 70 nm. In the mixed case when a coat with finite rigidity but increasing line tension is considered, a cup-to-sphere transition can occur for a line tension of 6 pN. The flat-to-curved and the cup-to-sphere transitions driven by line tension are both suppressed by high membrane tension.

1 Introduction

Clathrin-mediated endocytosis (CME) is the major pathway for bringing extracellular material into eukaryotic cells.[1] In CME clathrin triskelia form triple-coordinated lattices at the cytoplasmic side of the plasma membrane that drive inward vesicle budding. The process is initiated by adapter proteins like AP-2 that assemble at the cell membrane and trigger condensation of the clathrin triskelia.[2] Because clathrin triskelia have a built-in curvature and recruit additional proteins with an effect on membrane curvature, the membrane then tends to bend. After a clathrin-coated pit has formed, scission is effected by dynamin and a clathrin-coated vesicle is formed.[3,4] Despite many years of extensive study of CME, however, the exact physical nature of the invagination process is still elusive.[5–7]

Two paradigmatic models have been proposed to conceptualize the potential pathways of CME.[8] In the constant curvature model (CCM), the clathrin coat grows with a constant curvature presumably determined by the puckering angle of the clathrin triskelion.[9] Indeed *in vitro* assembly of pure clathrin lattices[10] and clathrin-coated vesicles[11] seem to suggest such a fixed preferred curvature, with a typical radius around 50 nm. In the constant area model (CAM), the clathrin coat first grows flat as a hexagonal lattice before it starts to bend.[12] Such a sequence of events suggests a larger role for cellular factors and indeed has recently been demonstrated in cell experiments.[13] It is further strengthened by the recent suggestion that flat clathrin lattices are less regular and more plastic than formerly appreciated.[14,15] A flat-to-curved transition implies that the projected radius decreases by a factor of up to 2, as observed experimentally.[13,15] The notion of plastic clathrin lattices is further strengthened by the recent finding that different cell types form flat or curved clathrin structures depending on small changes in the clathrin heavy chain amino acid sequence in the central hub region above the membrane.[16] This suggests that in general, cells can dynamically control spontaneous curvature, *e.g.* by mixing these different variants or by other changes in the same region, in particular by binding of additional proteins that affect curvature.

While for both CCM and CAM experimental evidence has been reported,[11–13,15,17] no simple theoretical model exists that allowed one to explore different pathways in one unifying framework. In order to address the question which invagination pathways might exist and which physical factors might favor one over the other, here we describe the invagination energetics using a membrane Hamiltonian that includes the main relevant contributions from both clathrin coat and plasma membrane. Our approach is conceptually similar to theoretical studies of the formation of curved membrane patches,[18] but addresses the specific questions relevant in the context of CME.

We start from the common assumption that the main energy source driving the growth process is polymerization of the clathrin coat.[11] Curvature generation is driven mainly by the

[a] *Institute for Theoretical Physics, Heidelberg University, Philosophenweg 19, 69120 Heidelberg, Germany. E-mail: schwarz@thphys.uni-heidelberg.de*
[b] *BioQuant, Heidelberg University, Im Neuenheimer Feld 267, 69120 Heidelberg, Germany*
† Present address: Department of Bionanoscience, Kavli Institute of Nanoscience, Delft University of Technology, Van der Maasweg 9, 2629 HZ Delft, The Netherlands.

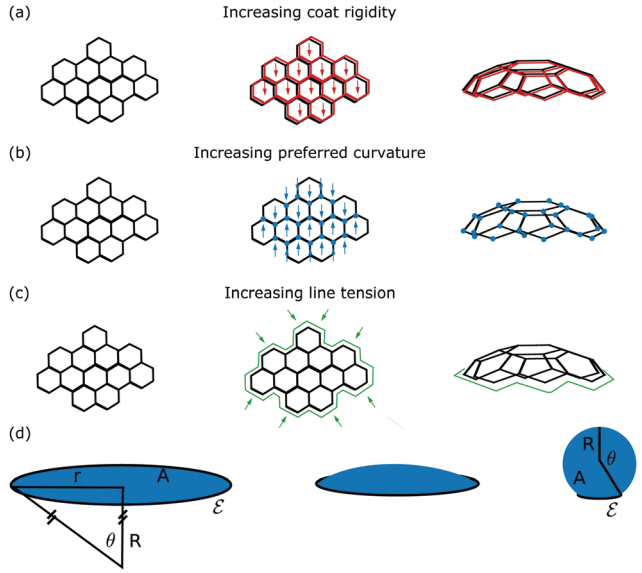

Fig. 1 Three physical mechanisms that can drive the invagination of clathrin coats. (a) Increasing clathrin coat density would increase the cost of bending away from the preferred curvature of the clathrin coat and thus force the lattice to bend. (b) Changing the internal structure of clathrin triskelia could change their preferred curvature and thus would increase the tendency of the lattice to bend. (c) Increasing line tension due to *e.g.* recruitment of specific factors to the edges of the clathrin coat would increase the cost of assembling flat clathrin coats. Since the overall energy could decrease by bending, an increasing line tension would force the lattice to bend. (d) All three cases can be modeled in a continuum theory with the same set of geometrical parameters. The clathrin-coated vesicles are characterized by area A, edge length $\mathscr{E}$, radius R and invagination angle θ. The radius r of the area-equivalent flat patch is a convenient coordinate for coat growth.

preferred curvature of the clathrin triskelia, which we include as preferred (or spontaneous) curvature into our membrane Hamiltonian.[19] Because it has been found experimentally that the density of clathrin lattices increases during the flat-to-curved transition,[20] we consider the possibility that an increase in coat bending rigidity can drive formation of curvature (Fig. 1a). Alternatively, we consider the possibility that the preferred curvature of clathrin triskelia can increase,[21] controlled by *e.g.* changes in the clathrin triskelia or binding of additional proteins, most likely in the central hub region (Fig. 1b). As a third option, we consider the possibility that an increase in line tension drives invagination (Fig. 1c), a mechanism which has been suggested before for vesicle formation after phase separation of membrane domains.[22] The line tension could originate *e.g.* from unbound clathrin binding sites at the edge of the clathrin coat, from additional proteins that preferentially bind at the edge of the clathrin coat or by lipid segregation in the membrane. We consider this scenario without and with coat rigidity. While the first two mechanisms (increase in coat stiffness or spontaneous curvature) couple to the bulk of the coat, the last two (increase in line tension without and with coat rigidity) couple to its rim.

In contrast to earlier work along these lines, we do not restrict vesicle radius to a fixed value,[11] as suggested by the CCM, but allow for a variable radius (Fig. 1d). Conveniently all four scenarios can be formulated in the same variables and therefore directly compared against each other. As we will show below, our theory can be formulated in analytical form and therefore is very transparent. Because here we choose a continuum approach, we do not explicitly model the exact coordination in the clathrin lattice, but implicitly assume that once energetics forces the lattice to bend, coordination will adapt correspondingly. This agrees with the recent suggestion that clathrin lattices are not as regular as assumed earlier.[14,15]

We use our theoretical framework to explore different pathways through the invagination process. For the rigidity-driven case, we find that coat rigidities around 30 k_BT are required for vesicle formation at low membrane tensions. In this case curvature occurs along with growth, *i.e.* similar to the CCM. For high membrane tensions this value has to increases to around 150 k_BT for vesicle formation during coat growth, since a constant stiffness would lead to stalled growth. For the preferred curvature-driven case, we find that coat radii of only around 200 nm are required for vesicle formation at low membrane tensions. In this case curvature occurs again with growth. For high membrane tensions the preferred radius has to decrease to around 70 nm for vesicle formation during coat growth. For invagination driven by line tension, around 6 pN are required for vesicle formation at low membrane tension with and without coat rigidity. In the case without coat rigidity we find a flat-to-curved transition of the coat, *i.e.* the coat has first grown flat to a certain size before curvature is acquired. The invagination occurs similar to the CAM, where clathrin coats do not grow anymore during the transition. In the case with finite coat rigidity we find a cup-to-sphere transition of the coat, *i.e.* the coat first grows curved to a certain size before it invaginates completely. For high membrane tension both transitions are suppressed.

2 Model

In order to model the assembly and invagination of clathrin coats, we consider the elastic energies of both coat and membrane. The driving force for growth is the polymerization energy of the clathrin coat, but the driving force for acquisition of curvature is less clear. We consider clathrin coats as circular protein domains closely coupled to the plasma membrane, with a similar energetics like lipid domains or rafts that are embedded in the plasma membrane.[22] The total energy is described by a generalization of the Helfrich bending Hamiltonian[23]

$$\mathscr{H} = \int_{\text{coat}} \left(-\mu + 2\kappa_c (H - H_0)^2\right) \mathrm{d}A + \int_{\text{mem}} \left(2\kappa H^2 + \sigma\right) \mathrm{d}A + \zeta \mathscr{E}. \quad (1)$$

The first integral extends over the coat area and contains the polymerization energy density of the clathrin coat μ and its stiffness κ_c. H is the mean curvature and H_0 the preferred (or spontaneous) curvature that clathrin triskelia impose onto the membrane. As κ_c or H_0 increases, the system would be forced to bend because it has to pay more energy for bending away from the preferred curvature H_0 (Fig. 1a and b).

The second integral extends over the membrane area and contains its bending rigidity κ and membrane tension σ. We assume that the membrane by itself tends to be flat (no preferred curvature). Membrane tension is known to be a central regulator of curvature in CME.[13,24] The last term introduces a line tension ζ that is conjugated to the edge length $\mathscr{E}$. The main effect of a line tension is to reduce the length of the rim. With conserved area, this should lead to bending (Fig. 1c), as known from vesicle budding.[11,22,25]

In eqn (1), the second integral over the membrane runs over a larger area than the first one over the coat, because it also has to include the free membrane that is not covered by the clathrin coat. However, by solving the shape equations for the free membrane, it has been shown recently that the energy of the free membrane only contributes up to 20% to the total energy of the membrane for axisymmetric membrane deformations around spherical particles.[26] In order to arrive at an analytical theory, in the following we neglect this part of the energy. Then the two integrals in eqn (1) run over the same area. In the following, we assume that the clathrin patch adopts the shape of a spherical cap, as found in particle-based computer simulations of membrane patches with spontaneous curvature.[18] With the spherical cap assumption, all the relevant energy contributions can be written in analytical form.

As shown in Fig. 1d, a spherical cap is characterized by radius of curvature R and opening angle θ. From this the area follows as $A = 2\pi R^2(1 - \cos\theta)$ and the edge length as $\mathscr{E} = 2\pi R \sin\theta$. The surface energy from eqn (1) now reads

$$E = -\mu A + 2\kappa_c(H - H_0)^2 A + 2\kappa H^2 A + \sigma\Delta A + \zeta\mathscr{E}. \quad (2)$$

The mean curvature is given by $H = 1/R$ and the preferred curvature of the clathrin coat is $H_0 = 1/R_0$, where R_0 is the preferred radius of the clathrin coat that is determined by the internal structure of the clathrin lattice. The membrane excess area ΔA can be calculated from the area difference between the spherical cap area and the corresponding (projected) flat circular area:

$$\begin{aligned}\Delta A &= A - \pi R^2 \sin^2\theta = A - \frac{\pi A \sin^2\theta}{2\pi(1-\cos\theta)} \\ &= A\left(1 - \frac{1-\cos^2\theta}{2(1-\cos\theta)}\right) = \frac{A}{2}(1-\cos\theta).\end{aligned} \quad (3)$$

Because the area A is the most important control parameter in our context, we choose to consider E as a function of A and θ rather than as a function of R and θ. We therefore write $R = \sqrt{A/(2\pi(1-\cos\theta))}$ and $\mathscr{E} = \sqrt{2\pi A(1+\cos\theta)}$. With these results and definitions, eqn (2) now reads

$$\begin{aligned}E &= -\mu A + 4\pi\kappa_c(1-\cos\theta)\left(1 - \sqrt{\frac{A}{2\pi R_0^2(1-\cos\theta)}}\right)^2 \\ &\quad + 4\pi\kappa(1-\cos\theta) + \frac{\sigma A}{2}(1-\cos\theta) + \zeta\sqrt{2\pi A(1+\cos\theta)}.\end{aligned} \quad (4)$$

The polymerization energy in eqn (4) drives the assembly of clathrin coats and both the bending and tension energies of the membrane favor the assembly of flat clathrin coats. In contrast, the main effect of coat rigidity, preferred curvature and line tension is to drive the invagination process. Thus our modelling approach immediately suggests several distinct pathways that can generate curvature.

In order to derive analytical solutions for this model, in the following we treat these competing pathways one after the other. First we investigate the case where the bending rigidity of the coat drives the invagination process. Here we assume a constant value for the preferred curvature and neglect the line tension. Second we consider the case where the preferred curvature drives the bending of the coat. Here we assume a constant value for the coat rigidity and again neglect the line tension. Third we investigate the case that the line tension drives the invagination in the absence of any coat rigidity or preferred curvature. Fourth we again consider the case that the line tension drives the invagination, but now with finite values for both coat rigidity and preferred curvature. Apart from this fourth case we do not treat more possible mixtures of the three fundamental physical pathways for invagination as this would clutter our theoretical analysis.

The parameter values that are used throughout this work are summarized in Table 1. For coat rigidity the upper value has been reported in the literature and here is taken as upper limit in the first case and as the parameter value in the second case. In the fourth case an intermediate value is taken. For preferred vesicle radius the lower value is taken as the parameter value in the first case and as the lower limit in the second case. In the fourth case the upper value is taken as the parameter value. For line tension the lower value has been reported in the literature and here is taken as lower limit.

There is experimental evidence that the density of clathrin triskelia increases during the transition from the flat to the curved state.[20] In addition, it was recently shown that flat clathrin lattices can be switched to a curved state by small changes in the clathrin heavy chain amino acid sequence in the central hub,[16] suggesting that changes to spontaneous curvature can also occur dynamically. Thus, the clathrin coat rigidity, the preferred curvature and the line tension are expected to change either upon increasing the clathrin density within the coat or by changing the internal state of clathrin triskelia. Therefore in the following we consider the coat rigidity κ_c, the preferred radius R_0 and the line tension λ not as constants but as dynamic parameters. Assuming that the clathrin coat equilibrates fast during coat formation, the system will relax to the state of global minimal energy in the absence of any energy barriers. With these assumptions, we can predict how the invagination develops with growth of the clathrin coat based on the energetics presented by eqn (4).

Table 1 Model parameters

Parameter	Used value	Ref.
Polymer energy density μ	0.11 mJ m^{-2}	11
Bending rigidity membrane κ	25 k_BT	27
Membrane tension σ	10^{-5}–10^{-4} N m^{-1}	28
Line tension ζ	5.2×10^{-2}–10 pN	11
Bending rigidity coat κ_c	0–300 k_BT	29
Preferred pit radius R_0	50–500 nm	11

3 Results

3.1 Variable coat rigidity

We first investigate the effect of coat stiffening as a potential mechanism to drive the invagination. To simplify the description and make the mechanism as transparent as possible, we keep the preferred curvature constant and neglect the line tension in this section, that is we set $R_0 = 50$ nm and $\zeta = 0$ in eqn (4). We treat the coat rigidity as a dynamic variable which can increase in time $\kappa_c = \kappa_c(t)$. However, we do not consider the dynamics of this change explicitly, since it is experimentally unknown.

We calculate the shape of clathrin coats determined by the minimum energy. In the model the coat shape is given by coat area A and invagination angle θ. We assume that the timescale of coat adaptation and invagination (dynamics in θ) will be small compared to the timescale of coat growth (dynamics in A). This assumption is motivated by the observation that the growth process takes several tens of seconds, whereas the clathrin exchange kinetics measured by fluorescence recovery after photobleaching is seconds, suggesting that the coat might adapt quite fast.[2] We conclude that in our model the coat assumes quasi instantaneously its minimal energy configuration in θ during the growth process.

In order to visualize the coat energy and to get an impression of how the invagination process proceeds, we plot the coat energy (given by eqn (4)) as a function of θ for two different coat rigidities in Fig. 2a. We find that depending on the coat rigidity either the curved state (marked by the arrow above the green curve) or the spherical state (marked by the arrow above the orange curve) defines the energy minimum. To determine if the curved or spherical state define the energy minimum we first determine the derivative of eqn (4) with respect to θ

$$\frac{\partial E}{\partial \theta} = \sin\theta\left\{\frac{\sigma}{2}A + 4\pi\left(\kappa_c\left(1-\frac{R}{R_0}\right)+\kappa\right)\right\} \stackrel{!}{=} 0. \tag{5}$$

First we note that eqn (5) can become zero either if the term in the brackets becomes zero or if $\theta = \pi$. For $\theta \to 0$ the expression stays finite, since $r = \theta R$ stays finite for $A > 0$. By using the expression of the spherical cap radius R, we can deduce from eqn (5) a quadratic equation for the radius r of a flat disc with the same area $A = \pi r^2$

$$r^2 - \frac{4\kappa_c}{R_0\sigma\sin\frac{\theta}{2}}r + \frac{8(\kappa+\kappa_c)}{\sigma} = 0, \tag{6}$$

which we can either solve for the invagination angle

$$\theta = 2\arcsin\left(\frac{4\kappa_c r}{R_0(\sigma r^2 + 8(\kappa+\kappa_c))}\right), \tag{7}$$

or for the radius

$$r = \frac{2\kappa_c}{R_0\sigma\sin\frac{\theta}{2}} \pm \sqrt{\left(\frac{2\kappa_c}{R_0\sigma\sin\frac{\theta}{2}}\right)^2 - \frac{8(\kappa+\kappa_c)}{\sigma}}. \tag{8}$$

Next, we calculate the second derivative of eqn (4)

$$\frac{\partial^2 E}{\partial\theta^2} = \cos\theta\left(\frac{\sigma}{2}A + 4\pi(\kappa+\kappa_c)\right) + \frac{\kappa_c}{R_0}\sqrt{2\pi A(1-\cos\theta)}, \tag{9}$$

implying a minimum for $\theta \leq \pi/2$ and a minimum or maximum for $\theta > \pi/2$. We now calculate the angle as a function of radius for which the type of the extremum changes, $\partial^2 E/\partial\theta^2 \stackrel{!}{=} 0$, which leads to the equation

$$\alpha\cos\theta + \beta\sin\frac{\theta}{2} = 0, \tag{10}$$

with $\alpha = \sigma r^2 + 8(\kappa + \kappa_c)$ and $\beta = 4\kappa_c r/R_0$. From eqn (6) we find $\alpha = \beta/\sin(\theta/2)$, relating the parameter values for which the extremum exists. Using this result on eqn (10) we get

$$\beta\left(\frac{\cos\theta}{\sin\frac{\theta}{2}} + \sin\frac{\theta}{2}\right) = 0. \tag{11}$$

Since eqn (11) can be solved only for $\theta = \pi$, the type of the extremum cannot change and eqn (8) defines the radius at which an invaginated state becomes an energy minimum.

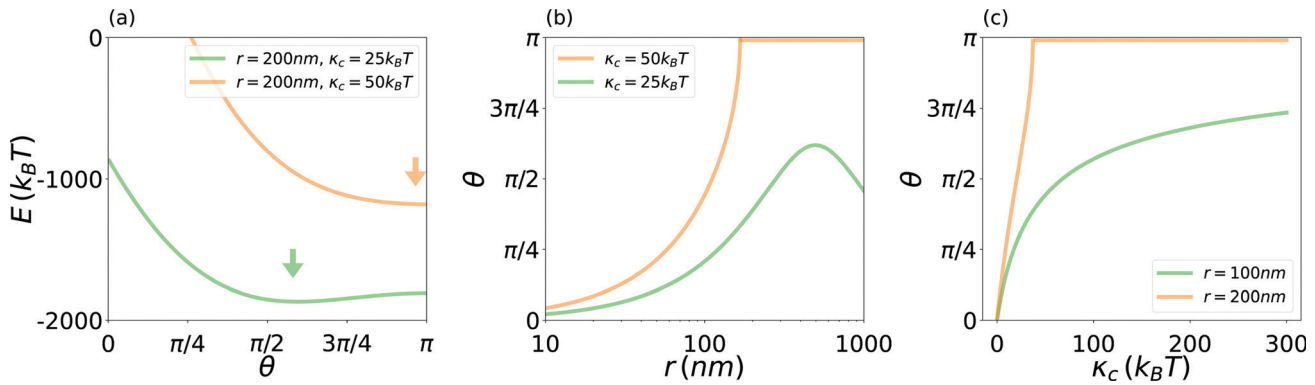

Fig. 2 Energies and invagination pathways for clathrin coats with variable coat rigidity κ_c, $R_0 = 50$ nm and $\sigma = 10^{-5}$ N m^{-1}. (a) The energy of clathrin coats with size $r = 200$ nm. For $\kappa_c = 25\ k_BT$ (green) the energy minimum is given for a curved state (green arrow), whereas for $\kappa_c = 50\ k_BT$ (orange) the spherical state becomes the energy minimum (orange arrow). (b) θ as a function of the radius r of the area-equivalent flat patch. For the smaller rigidity the coat only curves (green) while the coat becomes spherical for the larger rigidity (orange). (c) θ as a function of κ_c for two different values of r. Only for the larger radius the coat invaginates completely.

In Fig. 2b and c we show θ determined by eqn (7) as a function of the radius r of the area-equivalent flat patch ($A = \pi r^2$, *cf.* Fig. 1d) and coat rigidity κ_c, respectively. In the following, we use r as a convenient coordinate for growth. As expected, we find that the pathway of invagination is determined by the coat size and the coat rigidity. Importantly, the transition to the spherical state (orange) occurs continuously for an increasing coat size or coat rigidity.

To understand to which size clathrin coats grow we determine the derivative of eqn (4) with respect to A:

$$\frac{\partial E}{\partial A} = -\mu + \frac{\sigma}{2}(1-\cos\theta) + \frac{2\kappa_c}{R_0^2}\left(1 - \sqrt{\frac{2\pi R_0^2(1-\cos\theta)}{A}}\right) \stackrel{!}{=} 0. \tag{12}$$

The solution is given by

$$r = \frac{\sqrt{2R_0^2(1-\cos\theta)}}{1 - \frac{\mu R_0^2}{2\kappa_c} + \frac{\sigma R_0^2}{4\kappa_c}(1-\cos\theta)}. \tag{13}$$

The second derivative

$$\frac{\partial^2 E}{\partial A^2} = \frac{\kappa_c}{R_0^2}\sqrt{2\pi R_0^2(1-\cos\theta)}A^{-\frac{3}{2}}, \tag{14}$$

is always positive, thus eqn (13) defines an energy minimum. We now use the expression for the invagination angle, defined by eqn (7), in eqn (13) to determine the size to which clathrin coats will grow

$$r = \left(\sqrt{\frac{c_1^2}{4} - c_2} - \frac{c_1}{2}\right)^{1/2}, \tag{15}$$

where $c_1 = 16(\kappa + \kappa_c)/\sigma$ and $c_2 = 64(\kappa + \kappa_c)^2/\sigma^2 + 128\kappa_c^2(\kappa + \kappa_c)/(\sigma^2(\mu R_0^2 - 2\kappa_c)) < 0$.

The shape of clathrin coated structures is strongly determined by size, coat rigidity and membrane tension. Fig. 3 shows the state diagrams as a function of the coat radius r of the area-equivalent flat patch and coat rigidity κ_c for three different values of membrane tension σ. Because in this section we assume a finite and relatively large spontaneous curvature, the membrane will always be curved to a certain degree. We classify coats as flat for which the invagination angle is smaller than $\theta < 0.2\pi$ and as curved otherwise. Flat regions in the state diagrams are shown in white. Orange regions indicate the parameter space in which the spherical state is energetically favorable based on eqn (8) with $\theta = \pi$. Green regions indicate the parameter space in which the curved state is energetically favorable, using $\theta = 0.2\pi$ as dividing value in eqn (8). Finally the blue regions indicate the space in which clathrin coats will not grow anymore since they have reached their energy minimum determined by eqn (15).

Fig. 3a shows that for low membrane tension, clathrin coats get more and more curved as they grow and finally end up as spherical coats for large and intermediate coat rigidity. This is the typical growth behaviour in the CCM. For small coat rigidities clathrin coats get curved but do not transform to spherical coats. For increasing membrane tension, shown in Fig. 3b and c, the region in which spherical coats can form is reduced. Moreover, now the orange and green region are separated by the blue region, which indicates that although clathrin coats start to curve, they stop to grow before they reach the spherical shape. Only by increasing the coat rigidity one could drive a transition from the curved state to the spherical state.

3.2 Variable preferred curvature

Next we consider the effect of increasing preferred curvature of the clathrin coat as a potential mechanism to drive the invagination. To simplify the description and make the mechanism as transparent as possible, we now keep the coat rigidity constant and again neglect the line tension in this section, that is we set $\kappa_c = 300\ k_BT$ and $\zeta = 0$ in eqn (4). We treat the preferred radius of the clathrin coat as a dynamic variable, which can increase in time $R_0 = R_0(t)$. However, we do not consider the dynamics of this change explicitly, since it is experimentally unknown.

In Fig. 4a the energy of the coat (given by eqn (4)) is shown as a function of θ. Similar to before the clathrin coat only forms a

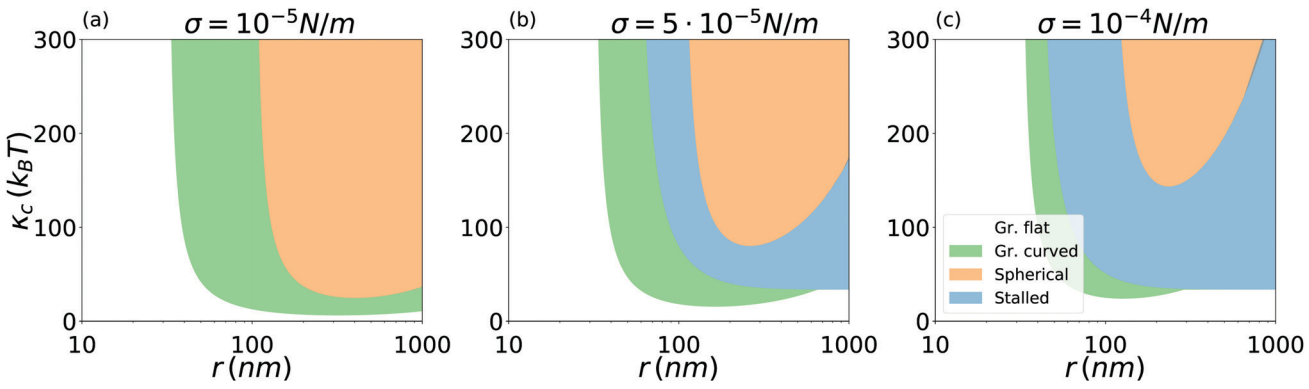

Fig. 3 State diagrams for invagination driven by variable coat rigidity. (a–c) State diagrams of clathrin coats as a function of the coat radius r of the area-equivalent flat patch and coat rigidity κ_c for three different values of membrane tension σ. The orange region indicates the parameter space where the spherical state is energetically favorable. In the green region the minimum energy state is curved ($\theta \geq 0.2\pi$) and in the white region the minimum energy state is flat ($\theta < 0.2\pi$). In the blue region clathrin coats do not grow.

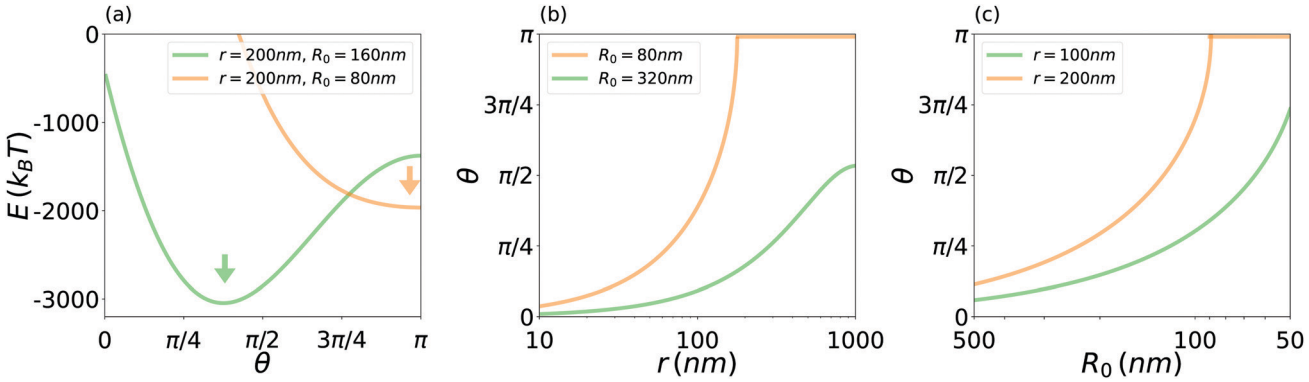

Fig. 4 Energies and invagination pathways for clathrin coats with variable preferred curvature $H_0 = 1/R_0$, $\kappa_c = 300\ k_BT$ and $\sigma = 10^{-5}$ N m^{-1}. (a) The energy of clathrin coats with size $r = 200$ nm. For $R_0 = 160$ nm (green) the energy minimum is given for a curved state (green arrow), whereas for $R_0 = 80$ nm (orange) the spherical state becomes the energy minimum (orange arrow). (b) θ as a function of the radius r of the area-equivalent flat patch. For the smaller value of the preferred curvature the coat only curves (green), while the coat becomes spherical for the larger value of the preferred curvature (orange). (c) θ as a function of R_0 for two different values of r. Only for the larger radius the coat invaginates completely.

sphere when the preferred curvature is large enough (marked by the arrow above the orange curve). Otherwise the coat will stay curved (marked by the arrow above the green curve). In Fig. 4b and c the invagination angle θ, determined by eqn (7), is shown as a function of the coat radius r of the area-equivalent flat patch and preferred radius. Again the transition to the curved state occurs continuously.

The equations, which we derived in the last section, also hold true in the case of constant coat rigidity but varying preferred curvature. Therefore, we use these equations to investigate shape as a function of the coat radius r of the area-equivalent flat patch, preferred radius and membrane tension in Fig. 5. As before, the orange region indicates the parameter space where the spherical state is energetically favorable based on eqn (8) with $\theta = \pi$. Similarly, the green region indicates the parameter space where the curved state is energetically favorable, where we use $\theta = 0.2\pi$ in eqn (8). In the white region flat clathrin coats are expected and in the blue region clathrin coats will not grow anymore since they have reached their energy minimum determined by eqn (15).

Comparing Fig. 5 to Fig. 3 we find qualitatively very similar results. For low membrane tension clathrin coats get more and more curved as they grow, *i.e.* we find the typical growth behaviour of the CCM (Fig. 5a). For increasing membrane tension (Fig. 5b and c), the orange and green region are separated by the blue region, which indicates that although clathrin coats start to curve they stop to grow before they reach the spherical shape. Only by increasing the preferred curvature one could drive a transition from the curved state to the spherical state. We note that our results agree with similar results that have been recently reported for membrane on which a preferred curvature is locally induced.[30]

3.3 Variable line tension without coat rigidity

We next investigate the effect of line tension as a potential mechanism to drive the invagination. For this purpose we treat the line tension as a dynamic variable $\zeta = \zeta(t)$. Since experimental details are unknown, however, we do not consider the dynamics explicitly. To simplify the description we neglect coat stiffening and preferred curvature of the clathrin coat in this section, that is we set $\kappa_c = 0$ and $H_0 = 0$ in eqn (4). The coat energy then reads

$$E = -\mu A + 4\pi\kappa(1 - \cos\theta) + \frac{\sigma}{2}A(1 - \cos\theta) + \zeta\mathscr{E}. \qquad (16)$$

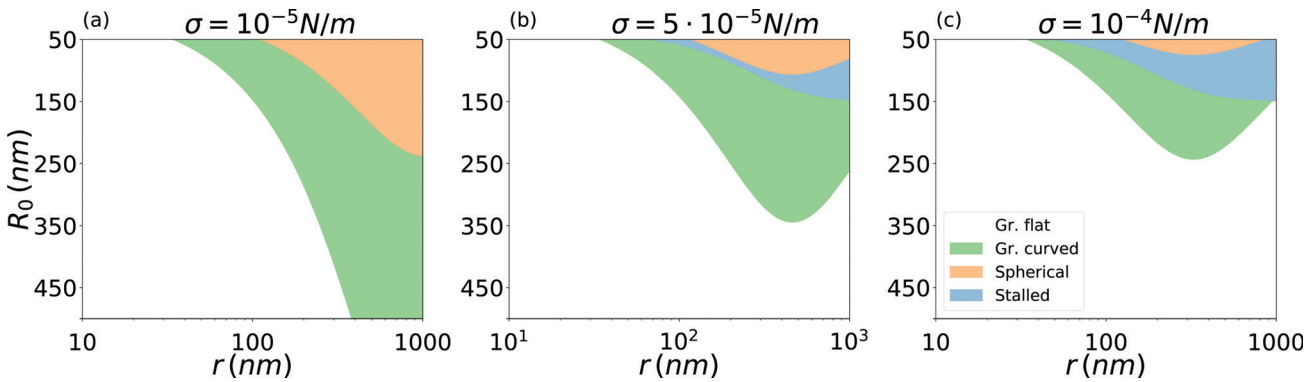

Fig. 5 State diagrams for invagination driven by variable spontaneous curvature. (a–c) State diagrams of clathrin coats as a function of the coat radius r of the area-equivalent flat patch and coat preferred radius R_0 for three different values of membrane tension σ. The orange region indicates the parameter space where the spherical state is energetically favorable. In the green region the minimum energy state is curved ($\theta \geq 0.2\pi$) and in the white region the minimum energy state is flat ($\theta < 0.2\pi$). In the blue region clathrin coats do not grow.

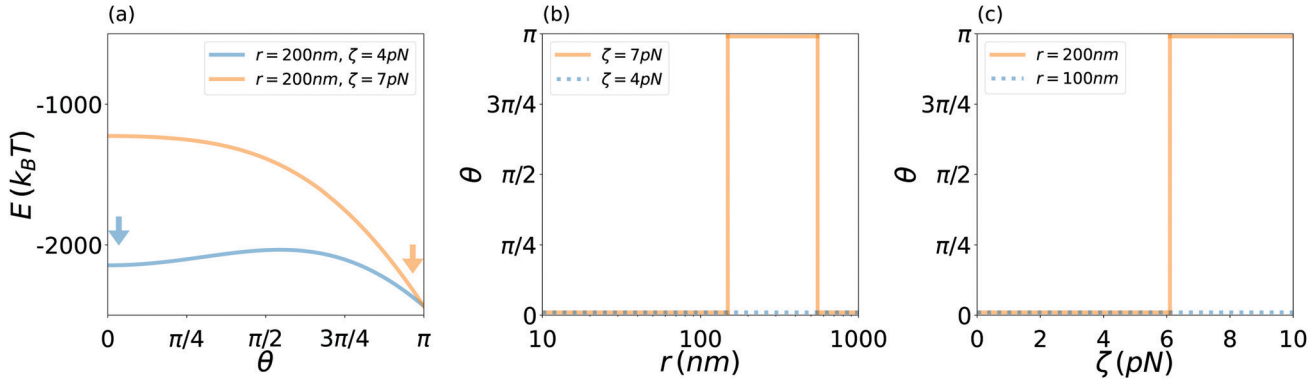

Fig. 6 Energies and invagination pathways for clathrin coats with variable line tension, no coat rigidity or preferred curvature, $\sigma = 10^{-5}$ N m^{-1}. (a) The energy of clathrin coats with size r = 200 nm and with a line tension of ζ = 4 pN (blue) and ζ = 7 pN (orange), respectively. For the lower value of the line tension the spherical state is the energy minimum. However, the coat is flat (blue arrow) because the flat state is separated from the spherical state by an energy barrier. For the larger value of line tension the energy barrier vanishes and the spherical state becomes the energy minimum (orange arrow). (b) θ as a function of the radius r of the area-equivalent flat patch. For the smaller value of line tension the coat stays flat and does not curve (blue), while the coat becomes spherical for the larger value of line tension (orange). (c) θ as a function of ζ for two different values of r. Only for the larger radius the coat invaginates completely, whereas it stays flat otherwise.

Fig. 6a shows the energy of eqn (16) as function of θ. For a line tension of 4 pN the spherical state is the energy minimum, however, separated from the flat state by an energy barrier such that the coat stays flat (marked by the arrow above the blue curve). For a line tension of 7 pN the energy barrier vanishes and the coat becomes spherical (marked by the arrow above the orange curve).

Next, we compare the energy of the flat coat to the spherical coat. By going to the double limit of a flat disc $\theta \to 0$, $R \to \infty$ and $r = R\theta$ finite, we find the disc energy

$$E_\mathrm{d} = -\mu\pi r^2 + \zeta 2\pi r, \tag{17}$$

with the disc area $A = \pi r^2$. For the sphere, on the other hand, where $\theta \to \pi$, R = const. and the same area A, the energy equals

$$E_\mathrm{s} = -\mu\pi r^2 + 8\pi\kappa + \sigma\pi r^2. \tag{18}$$

Next, we calculate the radius r for which the sphere becomes energetically favorable, $E_\mathrm{d} - E_\mathrm{s} = 0$, thus

$$r^2 - 2\frac{\zeta}{\sigma}r + 8\frac{\kappa}{\sigma} = 0. \tag{19}$$

Solving this equation for r we get

$$r = \frac{\zeta}{\sigma} \pm \sqrt{\left(\frac{\zeta}{\sigma}\right)^2 - 8\frac{\kappa}{\sigma}}. \tag{20}$$

This equation implies that a flat-to-curved transition can only occur if the line tension is sufficiently large.

We now determine the energy extrema of eqn (16)

$$\frac{\partial E}{\partial \theta} = \frac{\sigma}{2}A\sin\theta + 4\pi\kappa\sin\theta - \zeta\sqrt{\frac{\pi A(1-\cos\theta)}{2}} \stackrel{!}{=} 0. \tag{21}$$

Solving this equation we find an energy extremum for

$$\theta = 2\sec^{-1}\left(\frac{8\kappa\pi + \sigma A}{\zeta\sqrt{\pi A}}\right). \tag{22}$$

The extremum vanishes for $a \geq \sqrt{2}$, *i.e.* the line tension ζ and the coat area A determine whether the extremum vanishes or not. We calculate the size for which the extremum vanishes, *i.e.* $\theta = 0$

$$r^2 - \frac{\zeta}{\sigma}r + 8\frac{\kappa}{\sigma} = 0. \tag{23}$$

Solving this equation for r we get

$$r = \frac{\zeta}{2\sigma} \pm \sqrt{\left(\frac{\zeta}{2\sigma}\right)^2 - 8\frac{\kappa}{\sigma}}. \tag{24}$$

By calculating the second derivative of eqn (16) we determine the type of extremum that is given by eqn (22),

$$\left.\frac{\partial^2 E}{\partial\theta^2}\right|_{\theta=\theta^*} = \frac{1}{2}\left(\frac{\pi A\zeta^2}{A\sigma + 8\pi\kappa} - A\sigma - 8\pi\kappa\right). \tag{25}$$

Clearly, this equation becomes negative for small and large values of A, implying a maximum, *i.e.* an energy barrier. However, for intermediate values of A the equation can be larger than zero, implying a minimum in the energy landscape. Therefore, we determine the radius for which the type of the extremum changes $\partial^2 E(A)/\partial\theta^2|_{\theta=\theta^*} \stackrel{!}{=} 0$. Since we find eqn (24) again, the energy maximum would only switch to an energy minimum when the energy extremum vanishes completely. Therefore, either the flat state is an energy minimum, or the spherical state is an energy minimum, however, separated by an energy barrier from the flat state (determined by eqn (20)), or the spherical state is an energy minimum without energy barrier (determined by eqn (24)). Thus, the invagination of clathrin coats is either frustrated by a nucleation barrier or driven by spinodal decomposition, in agreement with recently reported results for a disk-to-vesicle transition of a membrane with line tension.[18]

Fig. 6b and c show the invagination angle (given by eqn (22)) as a function of the coat radius r of the area-equivalent flat patch and ζ for two values of coat size and line tension, respectively. For the smaller values of line tension and coat size, respectively,

the coats stay flat (blue). However, for the larger values of line tension and coat size the coat invaginates (orange). Importantly, in this case the transition from the flat coat to the spherical coat occurs discontinuously.

To complete the description we determine to which sizes clathrin coats grow, that is we determine the derivative of eqn (16) with respect to A:

$$\frac{\partial E}{\partial A} = -\mu + \frac{\sigma}{2}(1-\cos\theta) + \frac{\zeta}{2}\sqrt{2\pi(1+\cos\theta)}\frac{1}{\sqrt{A}}. \tag{26}$$

Since the second derivative of eqn (16) is negative everywhere

$$\frac{\partial^2 E}{\partial A^2} = -\frac{\zeta}{4}\sqrt{2\pi(1+\cos\theta)}\frac{1}{\sqrt{A^3}}, \tag{27}$$

the solution of eqn (26) defines an energy maximum given by

$$r = \frac{\zeta\sqrt{2(1+\cos\theta)}}{2\mu - \sigma(1-\cos\theta)}. \tag{28}$$

For a flat clathrin coat this simplifies to $r = \zeta/\mu$, which defines an initial energy barrier. After passing this barrier and the point where the coat energy crosses through zero ($E_d = 0$), defined through eqn (17), we have

$$r = \frac{2\zeta}{\mu}, \tag{29}$$

therefore flat coats can grow indefinitely, since the energy is only decreasing from that radius onwards.

In this section the shape of the clathrin coats is determined by coat size, line tension and membrane tension. Fig. 7 shows the state diagrams of clathrin coats as a function of the coat radius r of the area-equivalent flat patch and line tension for three values of membrane tension. Fig. 7a for low membrane tension shows that there exists an orange region of parameter space in which the spherical state is energetically favorable, as determined by eqn (24). In particular, we see that the line tension ζ needs to be above the value of 6 pN for the spherical solution to be stable. While in the blue region the clathrin coats are growing flat, in the white region the membrane stays bare since the initial barrier, determined by eqn (29), is too large.

Increasing the membrane tension as shown in Fig. 7b and c abolishes the region in which spherical coats are stable. Overall, Fig. 7 shows that clathrin coats can invaginate driven by an increasing line tension, but only when membrane tension is low. We note that this model variant is in agreement with a CAM, where the clathrin coat invaginates without further coat growth.

3.4 Variable line tension with finite coat rigidity

Because the case of variable line tension without coat rigidity and preferred curvature studied in the last section is instructive but not realistic, we finally explore a combination of the mechanisms from before, that is we now discuss the case of a variable line tension $\zeta = \zeta(t)$ with finite values for both coat rigidity and preferred curvature.

In this case we treat the full eqn (4) and set $\kappa_c = 50\ k_BT$ and $R_0 = 500$ nm, since we are interested in an intermediate situation that is not dominated by the rigidity of the clathrin coat. Fig. 8a shows the coat energy (given by eqn (4)) as function of θ for 300 nm and two different values of ζ. As expected, we now have a combination of the two mechanisms from before: for the smaller line tension we find that the global energy minimum is the spherical state, however, separated from the local energy minimum of a curved state by an energy barrier (marked by the arrow above the green curve). Because of this energy barrier the coat is expected to be curved. For the larger value of the line tension the intermediate energy barrier vanishes such that the coat is expected to be spherical (marked by the arrow above the orange curve). We note that a similar cup-to-vesicle transition has been recently described for a fluid membrane with preferred curvature and line tension.[18]

We now determine the energy extrema of eqn (4)

$$\frac{\partial E}{\partial \theta} = \sin\theta\left\{\frac{\sigma}{2}A + 4\pi\left(\kappa_c\left(1-\frac{R}{R_0}\right)+\kappa\right) - \zeta\sqrt{\frac{\pi A}{2(1+\cos\theta)}}\right\} \stackrel{!}{=} 0. \tag{30}$$

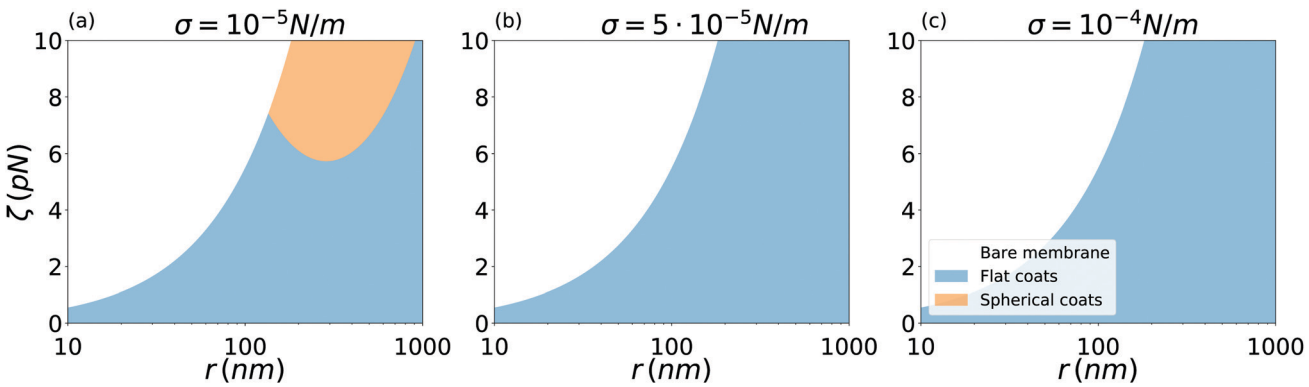

Fig. 7 State diagrams for invagination driven by variable line tension at vanishing coat rigidity. (a–c) State diagrams of clathrin coats as a function of the coat radius r of the area-equivalent flat patch and line tension ζ for three different values of membrane tension σ. The orange region indicates the parameter space where the spherical state is energetically favorable. In the blue region the minimum energy state is flat and coated, and in the white region the membrane is flat yet bare.

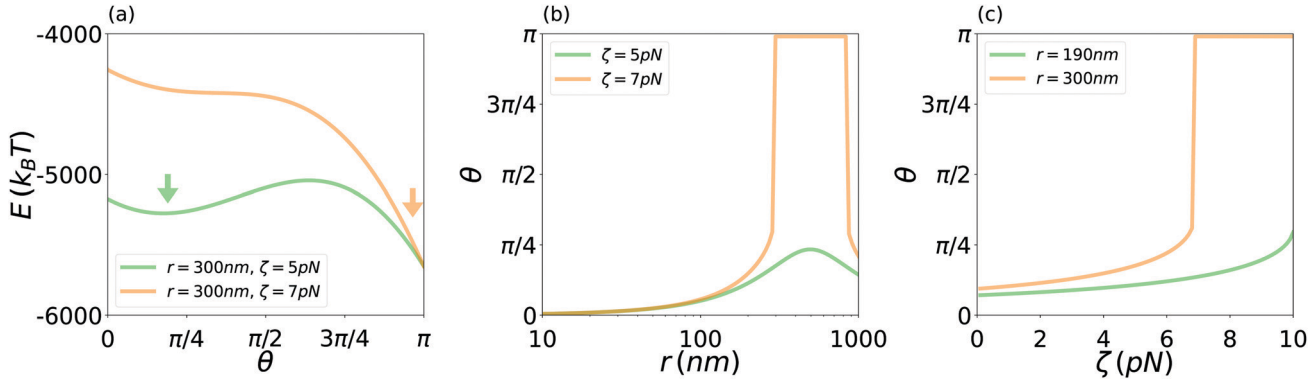

Fig. 8 Energies and invagination pathways for clathrin coats with variable line tension, $\kappa_c = 50\ k_BT$, $R_0 = 500$ nm and $\sigma = 10^{-5}$ N m^{-1}. (a) The energy of clathrin coats with size of $r = 300$ nm and with a line tension of $\zeta = 5$ pN (green) and $\zeta = 7$ pN (orange). For the lower value of line tension the curved state is the energy minimum (green arrow), while for the larger value of line tension the spherical state becomes the energy minimum (orange arrow). (b) θ as a function of the radius r of the area-equivalent flat patch. For the smaller value of line tension the coat stays curved (green), while the coat becomes spherical for the larger value of line tension (orange). (c) θ as a function of ζ for two different values of r. Only for the larger radius the coat invaginates completely.

Eqn (30) can be simplified to

$$\frac{\pi}{2}\sin\theta\left\{1-\frac{\beta}{\alpha}\frac{1}{\sin(\theta/2)}-\frac{\gamma}{\alpha}\frac{1}{\cos(\theta/2)}\right\}\stackrel{!}{=}0, \tag{31}$$

with $\alpha = \sigma r^2 + 8(\kappa_c + \kappa)$ $\beta = 4\kappa_c r/R_0$ and $\gamma = \zeta r$. Expanding eqn (31) around $\theta = 0$ and $\theta = \pi$ shows that eqn (31) < 0 for both $\theta \to 0$ and $\theta \to \pi$. Thus, eqn (31) can have two or one solutions, implying that a curved state is the energy minimum, or no solution implying that the spherical state is the energy minimum.

Since eqn (31) cannot be solved analytically, we solve it numerically. Fig. 8b shows θ as a function of the coat radius r of the area-equivalent flat patch, computed from eqn (31), corresponding to the minimal energy coat configuration. For the lower value of the line tension (green), we find that the coat is either flat ($\theta < 0.2\pi$) or curved ($\theta > 0.2\pi$). For the higher value of the line tension we also find a transition to the spherical state (orange). As expected, this transition is first continuous and then discontinuous since both the coat rigidity and the line tension drive the invagination. Fig. 8c shows θ as a function of ζ, computed from eqn (31). We find the same behaviour as in Fig. 8b: For the smaller value of r the coat stays flat or curved for all values of ζ, while it becomes spherical for the larger r at a certain ζ.

To complete the description we next compute the size to which coats grow by determining the derivative of eqn (4) with respect to A:

$$\frac{\partial E}{\partial A} = -\mu + \frac{\sigma}{2}(1-\cos\theta) + \frac{\zeta}{2}\sqrt{2\pi(1+\cos\theta)}\frac{1}{\sqrt{A}} + \frac{2\kappa_c}{R_0^2}\left(1-\frac{R_0}{R}\right). \tag{32}$$

By using the solution computed from eqn (31) on eqn (32), we can determine if a coat still grows (when eqn (32) is negative) or if the growth is stalled (when eqn (32) is positive).

In this section we explore how the invagination pathway of clathrin coats with constant rigidity is dictated by coat size, line tension and membrane tension. Fig. 9 shows the state diagrams of clathrin coats as a function of the coat radius r of the area-equivalent flat patch and ζ for three values of membrane

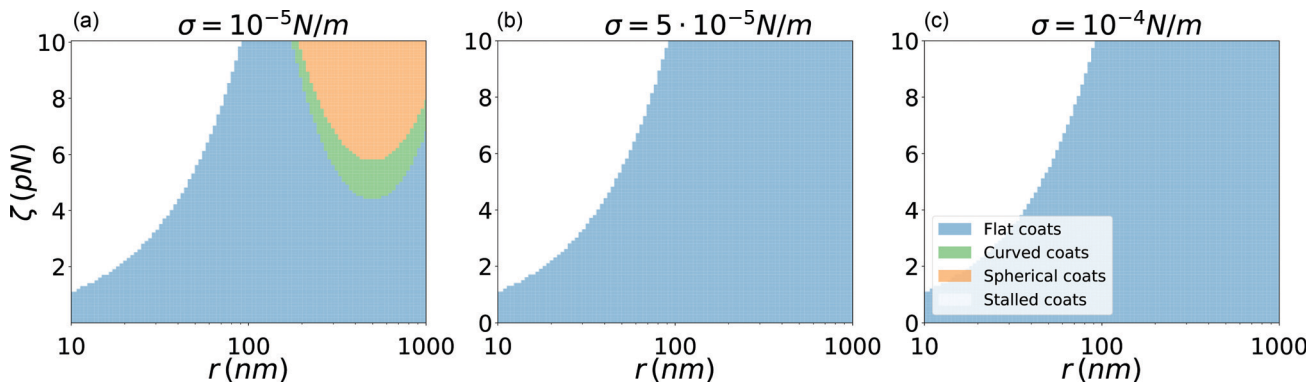

Fig. 9 State diagrams for invagination driven by variable line tension at finite coat rigidity. (a–c) State diagrams of clathrin coats as a function of the coat radius r of the area-equivalent flat patch and line tension ζ for three different values of membrane tension σ. The orange region indicates the parameter space where the spherical state is energetically favorable. In the green region the coat is curved, while it stays flat in the blue region. In the white region the coat growth is stalled.

tension. Fig. 9a for low membrane tension shows that the clathrin coat can be flat (blue region), curved (green region) or spherical (orange region), determined by eqn (31) and dependent on the combination of coat size and line tension. Moreover, the growth of clathrin coats is stalled (white region), determined by eqn (32). In addition, to the case without constant coat rigidity (*cf.* Fig. 7a) now also curved clathrin coats occur (green region). Therefore, clathrin coats first curve continuously before the transition to the spherical state occurs discontinuously.

By increasing the membrane tension as shown in Fig. 9b and c only flat and stalled clathrin coats occur and the transition to the spherical state is frustrated. To conclude, when considering the invagination pathway of clathrin coats that exhibit a variable line tension and a constant coat rigidity, we find that clathrin coats first curve steadily before a cup-to-sphere transition[18] occurs and the coats leap to the completely invaginated spherical state.

4 Discussion

Although it becomes increasingly clear that clathrin lattices can first assemble flat before they start to curve,[12,13,15,17] it is still elusive how the flat-to-curved transition works on a microscopic level and which factors determine which physical route is taken in detail. Light microscopy still lacks the spatial resolution to elucidate the dynamics of clathrin lattice reorganization and electron microscopy techniques lack the information on the time domain of clathrin coat rearrangements.[3] Thus, in this work we theoretically investigate the assembly and invagination of clathrin coats on the plasma membrane driven the competing physical mechansims of an increase in coat stiffness, preferred curvature and line tension.

Rather than providing a microscopic description of coat organization, *e.g.* by particle based computer simulations,[31–33] we take a continuum approach based on energetics and treat the clathrin coat as a protein domain closely coupled to the plasma membrane. We investigate four scenarios where coat invagination is driven by an increase in coat rigidity, preferred curvature or line tension. Our theory is completely analytical and reveals a rich landscape of possible invagination scenarios. While we find for coat stiffening and increasing preferred curvature that curvature occurs along with growth, for line tension the lattice must have grown to a certain size before curvature can be generated. In the case of a finite coat rigidity but increasing line tension, the coat first grows curved to a certain size before it completely invaginates. In addition, the line tension has to increase gradually in order to drive both the flat-to-curved transition and the cup-to-sphere transition. Very importantly, all of these processes depend strongly on membrane tension. For high membrane tensions, the flat-to-curved and the cup-to-sphere transitions are completely suppressed.

Our results on the influence of membrane tension on CME and in particular the flat-to-curved transition agree with experimental[13,24,34] and theoretical results[35,36] obtained earlier. Importantly, all mechanisms discussed here are compatible with the notion that the clathrin coat is initially flexible and plastic.[14,15,22] This initial state of the clathrin coat might resemble a liquid gel or fluid in which lattice reorganization is still possible.[22,37] Only as soon as the clathrin coated membrane starts to invaginate, the coat solidifies and the preferred curvature of the coat is fixed, effectively acting as a plastic ratchet.[38]

In extension to earlier work, our results predict that a flat-to-curved transition can occur as a consequence of increasing line tension, whereas for increasing preferred curvature or coat rigidity, curvature would increase gradually along with growth.[36] The notion that a flat-to-curved transition can occur as a result of an increasing line tension or preferred curvature of the clathrin coat was already discussed in the work of Lipowsky[22] and Gompper and coworkers.[21] The latter work explains the formation of invaginated clathrin lattices as an example of a two-component fluid in which a crystalline membrane patch, embedded in the plasma membrane, buds. In contrast to,[21] we here also considered the case where the bending energy of the coat increases due to an increase of the bending rigidity rather than an increase of preferred curvature. Moreover, we present an analytical theory that does not require computer simulations.

The size of clathrin cages assembled *in vitro* is smaller than the size of clathrin coats assembled on a membrane.[2,10] In other words the preferred curvature of clathrin triskelia without membranes differs from that of clathrin triskelia in clathrin coats assembled at the membrane. The origin of this striking difference is still unknown. It is likely that not only does the membrane constitute a larger resistance to clathrin bending, but also that the preferred curvature of clathrin triskelia is only set by their interplay with adaptor proteins and with other clathrin triskelia in the clathrin lattice.[39] For simplicity, here we have assumed well-defined values for the preferred curvature, similar to the approach taken when considering curved membrane patches.[18] As more experimental details are revealed on the clathrin system, the preferred curvature might has to be written as a function of the other system variables.

For the clathrin coats a constant polymerization energy μ was assumed (*cf.* Table 1).[11] However, one could speculate that clathrin coats that can grow denser exhibit an increasing binding energy and therefore also polymerization energy could be variable. This effect would not change the invagination pathway, however, it would change the size when the growth of a clathrin coat is energetically unfavorable, and hence stalled. Eqn (15), (29) and (32) predict that by increasing μ the region for which one finds stalled growth would decrease. In addition, one could also speculate that the clathrin binding energy changes with the invagination angle. In order to adequately address such a mechanism, however, more insight is required from the experimental side, so that this question can only be dealt with in future work.

Because we focus on local mechanisms to bend the membrane, we do not consider the potential mechanism of membrane bending by actin polymerizing in the cytoplasm.[40] Although present also in animal cells, this mechanism is much more relevant in cells like yeast, which have a large turgor pressure. In the future, these two research directions should be combined into a comprehensive framework.

To conclude, our approach provides a simple description of the shape changes of assembling clathrin coats based on a

transparent and analytically solvable continuum model. We lay out the three main physical pathways which can be driven by changes to the coat organization during growth. In the future, our model can be extended into the time domain using the assumption of overdamped dynamics. Here however time-resolved experimental data (*e.g.* on invagination angle and radius of curvature) would be very helpful as guide through the rich assembly landscape that becomes evident already in our simple continuum approach.

Conflicts of interest

There are no conflicts to declare.

Acknowledgements

F. F. acknowledges financial support by the Heidelberg Graduate School For Physics (HGSFP). U. S. S. acknowledges support as a member of the Interdisciplinary Center for Scientific Computing (IWR) and the Collaborative Research Center 1129 of the German Research Foundation (DFG) funded under Projektnummer 240245660.

References

1 B. Alberts, *Molecular biology of the cell*, Garland Science, New York, 6th edn, 2015.
2 M. Kaksonen and A. Roux, *Nat. Rev. Mol. Cell Biol.*, 2018, 313–326.
3 A. Picco and M. Kaksonen, *Curr. Opin. Cell Biol.*, 2018, **53**, 105–110.
4 M. Mettlen, P.-H. Chen, S. Srinivasan, G. Danuser and S. L. Schmid, *Annu. Rev. Biochem.*, 2018, **87**, 871–896.
5 M. Lampe, S. Vassilopoulos and C. Merrifield, *J. Struct. Biol.*, 2016, **196**, 48–56.
6 K. A. Sochacki and J. W. Taraska, *Trends Cell Biol.*, 2019, **29**, 241–256.
7 F. Baschieri, K. Porshneva and G. Montagnac, *J. Cell Sci.*, 2020, **133**, jcs240861.
8 V. Haucke and M. M. Kozlov, *J. Cell Sci.*, 2018, **131**, jcs216812.
9 T. Kirchhausen, *Curr. Opin. Struct. Biol.*, 1993, **3**, 182–188.
10 A. Fotin, Y. Cheng, P. Sliz, N. Grigorieff, S. C. Harrison, T. Kirchhausen and T. Walz, *Nature*, 2004, **432**, 573–579.
11 M. Saleem, S. Morlot, A. Hohendahl, J. Manzi, M. Lenz and A. Roux, *Nat. Commun.*, 2015, **6**, 6249.
12 O. Avinoam, M. Schorb, C. J. Beese, J. A. Briggs and M. Kaksonen, *Science*, 2015, **348**, 1369–1372.
13 D. Bucher, F. Frey, K. A. Sochacki, S. Kummer, J.-P. Bergeest, W. J. Godinez, H.-G. Kräusslich, K. Rohr, J. W. Taraska and U. S. Schwarz, *et al.*, *Nat. Commun.*, 2018, **9**, 1109.
14 F. Frey, D. Bucher, K. A. Sochacki, J. W. Taraska, S. Boulant and U. S. Schwarz, *New J. Phys.*, 2020, **22**, 073043.
15 K. A. Sochacki, B. L. Heine, G. J. Haber, J. R. Jimah, B. Prasai, M. A. Alfonzo-Mendez, A. D. Roberts, A. Somasundaram, J. E. Hinshaw and J. W. Taraska, *bioRxiv*, 2020, DOI: 10.1101/2020.07.18.207258.
16 G. Moulay, J. Lainé, M. Lemaître, M. Nakamori, I. Nishino, G. Caillol, K. Mamchaoui, L. Julien, F. Dingli, D. Loew, M. Bitoun, C. Leterrier, D. Furling and S. Vassilopoulos, *J. Cell Biol.*, 2020, **219**, e201912061.
17 B. L. Scott, K. A. Sochacki, S. T. Low-Nam, E. M. Bailey, Q. Luu, A. Hor, A. M. Dickey, S. Smith, J. G. Kerkvliet and J. W. Taraska, *et al.*, *Nat. Commun.*, 2018, **9**, 419.
18 H. Noguchi, *J. Chem. Phys.*, 2019, **151**, 094903.
19 A. Banerjee, A. Berezhkovskii and R. Nossal, *Biophys. J.*, 2012, **102**, 2725–2730.
20 K. A. Sochacki, A. M. Dickey, M.-P. Strub and J. W. Taraska, *Nat. Cell Biol.*, 2017, **19**, 352–361.
21 T. Kohyama, D. Kroll and G. Gompper, *Phys. Rev. E: Stat., Nonlinear, Soft Matter Phys.*, 2003, **68**, 061905.
22 R. Lipowsky, *J. Phys. II*, 1992, **2**, 1825–1840.
23 W. Helfrich, *Z. Naturforsch., C: Biosci.*, 1973, **28**, 693–703.
24 S. Boulant, C. Kural, J.-C. Zeeh, F. Ubelmann and T. Kirchhausen, *Nat. Cell Biol.*, 2011, **13**, 1124–1131.
25 A. Banerjee, A. Berezhkovskii and R. Nossal, *Phys. Biol.*, 2016, **13**, 016005.
26 F. Frey, F. Ziebert and U. S. Schwarz, *Phys. Rev. E*, 2019, **100**, 052403.
27 G. Kumar and A. Sain, *Phys. Rev. E*, 2016, **94**, 062404.
28 L. Foret, *Eur. Phys. J. E: Soft Matter Biol. Phys.*, 2014, **37**, 42.
29 A. J. Jin, K. Prasad, P. D. Smith, E. M. Lafer and R. Nossal, *Biophys. J.*, 2006, **90**, 3333–3344.
30 Y. A. Omar, A. Sahu, R. A. Sauer and K. K. Mandadapu, *Biophys. J.*, 2020, **119**, 1065–1077.
31 W. K. den Otter and W. J. Briels, *Traffic*, 2011, **12**, 1407–1416.
32 R. Matthews and C. N. Likos, *Soft Matter*, 2013, **9**, 5794–5806.
33 M. Giani, W. den Otter and W. Briels, *J. Chem. Phys.*, 2017, **146**, 155102.
34 N. Willy, J. Ferguson, S. Huber, S. Heidotting, E. Aygün, S. Wurm, E. Johnston-Halperin, M. Poirier and C. Kural, *Mol. Biol. Cell*, 2017, **28**, 3480–3488.
35 J. E. Hassinger, G. Oster, D. G. Drubin and P. Rangamani, *Proc. Natl. Acad. Sci. U. S. A.*, 2017, **114**, E1118–E1127.
36 L. Foret, *Physics of Biological Membranes*, Springer International Publishing, Cham, 2018, pp. 385–419.
37 N. Cordella, T. J. Lampo, N. Melosh and A. J. Spakowitz, *Soft Matter*, 2015, **11**, 439–448.
38 L. Hinrichsen, A. Meyerholz, S. Groos and E. J. Ungewickell, *Proc. Natl. Acad. Sci. U. S. A.*, 2006, **103**, 8715–8720.
39 W. F. Zeno, J. B. Hochfelder, A. S. Thatte, L. Wang, A. K. Gadok, C. C. Hayden, E. M. Lafer and J. C. Stachowiak, *bioRxiv*, 2020, DOI: 10.1101/2020.06.04.134080.
40 S. Dmitrieff and F. Nédélec, *PLoS Comput. Biol.*, 2015, **11**, e1004538.